PCCP

Accepted Manuscript

ROYAL SOCIETY OF CHEMISTRY

www.rsc.org/pccp

Journal Name

Broadband two dimensional infrared spectroscopy of cyclic amide 2-Pyrrolidinone

Kiran Sankar Maiti[a][†]

In the past one and a half decades there has been a significant methodological and technological development of two dimensional infrared (2DIR) spectroscopy which unfolds many underlying physical and chemical processes of complex molecules, especially for biological molecules. Due to the extreme technical difficulties and non uniform performance of ultrafast laser, so far, the method is mostly applied to a small spectral region. A rather simple experimental methodology is presented here which is capable to cover a broad spectral range from $1500\,cm^{-1}$ to $3500\,cm^{-1}$ to explore the molecular structure of cyclic amide, 2-Pyrrolidinone via the time-resolved coupling of CO, CH and NH stretch vibrations. The signature of the coherent as well as incoherent coupling have been found. The amide-I band is incoherently coupled to the CH and NH stretch vibrations and acts as an acceptor mode for the vibrational energy relaxation from the CH and NH stretch vibrations.

1 Introduction

Many important chemical and biological activities are triggered by the fast molecular conformational changes in the condensed phase[1–6]. Molecular vibrational frequencies in condensed phase are not only sensitive to the molecular bond connectivity but also sensitive to solute/solvent interactions[7]. The local and non-local interactions to the vibrational band of the molecule, make it extremely difficult to understand the structure and the fast dynamics of the molecule[8–12]. A significant efforts have been devoted for last couple of decades to develop tools to monitor the three dimensional molecular conformations in real time. Among many powerful techniques, recently developed two dimensional infrared spectroscopy (2DIR)[13–15], which has essentially unlimited time resolution on the scale of large molecular motions, is one of the most promising techniques to visualize the structural changes in complex molecules[16–21].

Since one-and-half decade, there have been a handful of technical and theoretical developments on the multidimensional IR techniques[22–32] and now a days these are routinely using as a tool for studying the structure and ultrafast dynamics of biological molecules[33–40]. Most of them are restricted to investigate spectrally one or few near by vibrational modes of the molecule, which only provide partial information about the structure of the molecule. Due to its extremely technical difficulties, still the technique is fairly remote to explore the full molecular picture[41]. Additionally laser intensity drops very fast at low frequency region[42], which limits the applicability of the technique to disentangle the low frequency bending modes of the molecule. In a recent work, Zheng's group able to collect a wide frequency region using multiple-mode 2DIR spectroscopy[43]. They synchronized a picosecond and a femtosecond amplifier with the single seed laser to produce narrow pump and wide probe beam with reasonably high pulse energy. The technique is fair enough to cover low frequency mode, but due to the picosecond pump pulse, it has limited application to follow the fast molecular motion. A rather simple experimental technique which can cover a fairly wide spectral range ($1500\,cm^{-1}$ to $3600\,cm^{-1}$) to reveal most of the vibrational band of the biomolecules using femtosecond pump and probe pulses is presented in this article. In the experiment collinear pump pulses pair are used to excite the molecules and probe with a non-collinear laser pulse, absorptive spectra has been collected[44].

In this work 2-Pyrrolidinone molecule is selected as a model molecule, which has most of the signature of the protein and the peptide. Additionally its hydrogen bond characteristic allows one to study the structural sensitivity with hydrogen bonding, which is a prominent feature of the biomolecules. Its structure and the hydrogen bonded oligomers are presented in Fig. 1. 2-Pyrrolidinone is a fairly moderate size molecule for reasonably accurate ab initio calculation[45]. The C=O double bond structure serves as model system for protein back bone amide-I band and the NH bond allows to study the amide-A band in protein and peptide.

[a] Address, Lehrstuhl für Physikalische Chemie, Technische Universität München, D-85747 Garching, Germany; E-mail: kiran.maiti@ch.tum.de
[†] 'Present address:' Universität Bayreuth, Universitätsstraße 30, D-95447 Bayreuth, Germany.
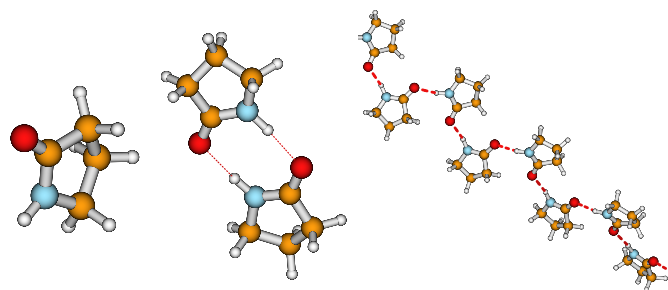
Fig. 1 Structure of 2-Pyrrolidinone molecule and its hydrogen bonded oligomers. The dashed line indicates the intermolecular hydrogen bonding. (a) Monomer, (b) doubly hydrogen bonded dimer (DHBD) (c) hydrogen bonded molecular chain.

Fig. 2 Schematic diagram of the experimental setup for 2DIR spectroscopy in pump-probe geometry. The beam geometry is depicted in inset.

2 Experimental procedures

Femtosecond regenerative/multi-pass Ti:Sapphire amplifier (Integra-C, Quantronix) is used to obtain an initial femtosecond pulses at $800\,nm$. The output of the Integra-C is $100\,fs$ transform-limited $2.5\,mJ$ pulses at a $1\,kHz$ repetition rate. The amplified beam is split into two beams $(40:60)$ and used to pump two traveling-wave optical parametric amplifiers (TOPAS, Light conversion). Along with the non-collinear difference frequency generator (NDFG, Light conversion) one of the TOPAS creates tunable (from $2.8\,\mu m$ to $12\,\mu m$) pump beam and other TOPAS produces independently tunable (from $2.8\,\mu m$ to $12\,\mu m$) probe beam, providing a combination that will permit to perform the two colour experiment in a broadband spectral range. The shot-to-shot IR instability is less than $1\,\%$ and the long term stability is such that data can be collected continuously for several days.

The pump beam is split into two beams (pulse-I and pulse-II) to produce two pump pulses for two dimensional echo experiment in pump-probe geometry (see Fig. 2). Both the pump pulses are reflected back from two retroreflectors placed on two independently computer controlled translation stages which creates the time delay between different pulses. The pulse-I passes through two calcium fluoride (CaF_2) wedges, placed in such a way that the pulse-I travels in the same direction after transversing through two wedges. One of the wedge is placed on a computer controlled translation stage to create a desirable phase difference from second pump pulse (pulse-II). Both the pump pulses are then overlapped by using a zinc selenide (ZnSe) beam splitter, so that they can propagate collinearly and then focuss on the sample by an off axis parabolic mirror. The probe pulse (pulse-III) is also focussed on the sample using the same off axis parabolic mirror and crosses the pump pulse inside the sample with a small angle (about $12\,°$).

2-Pyrrolidinone (C_4H_7NO) is purchased from Sigma-Aldrich with $99.9\,\%$ purity and dissolved in CCl_4 ($99.9\,\%$) with out any further purification. The concentration of the sample is optimized to $20\,\%$ by volume to perform the experiment across the broad spectral region with a reasonable signal strength. The sample is held in between two CaF_2 plates separated by a $15\,\mu$
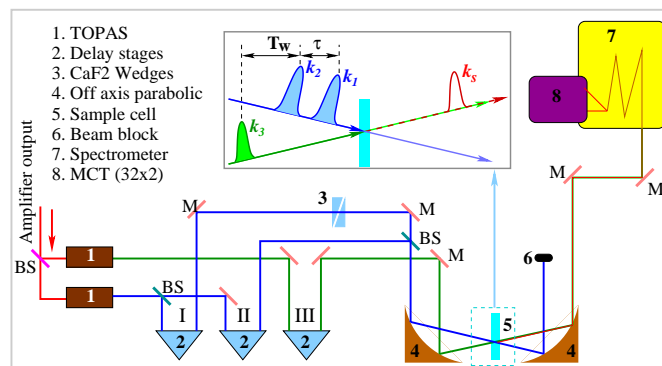
teflon spacer. The peak absorption of the sample is $\sim30\,\%$ at the NH stretch vibrational band region. All the experiments have been performed at room temperature $(21\,°\mathrm{C})$. The whole system is purged with dry air to remove the water vapor from the system.

To produce and detect the echo signal one of the pump pulses (Pulse-II) is chopped by a $500\,\mathrm{Hz}$ optical chopper from New Focus. The vibrational echo signal is created inside the sample due to the interections of three excitation pulses and emitted in the same direction as the probe beam. The probe beam itself acts as a local oscillator (LO) in the self-heterodyne-detection of the echo signal. The signal is spectrally resolved using the Horiba Jobin Yvon iHR320 spectrometer and is detected by a 64 elements MCT double array (from Infrared Systems Development). 0 to 31 elements are used to detect the reference signal and 32 to 63 elements are used to detect the echo signal. At each monochromator setting, both the arrays detect 32 individual wavelengths. The reference signal is used to compensate the shot-to-shot fluctuation of the IR pulse.

The phase-resolved, heterodyne detected, vibrational echo is measured as a function of the monochromator frequency, ω_m, and two time variables, τ and T_w that are defined as the time between the first and second interactions and the second and third interactions, respectively. In the experiment, τ variable is scanned in $1\,fs$ to $3\,fs$ time steps depending upon the spectral region of interest. The phase of the echo electric field is scanned relative to the fixed local oscillator electric field, resulting in an interferogram measured as a function of the τ variable. The interferogram contains the amplitude, sign, frequency and phase of the vibrational echo electric field as it varies with τ. By the Fourier transformation, this interferogram is converted into the frequency variable ω_τ.

The measured signal is the square of the sum of the vibrational echo electric field, S, the pump-probe signal of the pulse-I and pulse-II and the local oscillator electric field. The pulse-II is chopped at a rate of $500\,\mathrm{Hz}$, then subtracting the chopped signal from the unchopped signal, practically the local oscillator electric field and the pump-probe signal from the pulse-I are removed.

After the Fourier transformation of τ, the low frequency pump-probe signal of the pulse-II is separated from the high frequency echo spectra.

The crucial requirement for the broadband 2DIR spectroscopy is sufficient laser power in a broad spectral range, which is possible with a careful choice of the pump laser power for the white light generation in OPA. The optimal pump power along with careful choice of the crystal angle provides a nearly uniform power IR laser beam in a broad spectral range. Another advancement of this spectroscopic setup is the use of translating CaF_2 wedge along with high resolution delay stage which provides a perfect phase matching conditions between different laser pulses. These two simple modifications makes the spectrometer efficient to collect the 2DIR spectra of biological molecules over a broad spectral region.

3   Results and Discussions

Two dimensional vibrational echo spectra, taken in the pump-probe geometry is presented here. The broad band echo spectra in Fig. 3 is constructed by nine quadrants, representing all the combinations of CO, CH and NH bands. The quadrants are separated by the dashed lines. The white gap in the spectra indicates broken frequency axis. The red colour contour represents the positive peak and the negative peak is represented by the blue colour contour. The quadrants are named with pump first and then probe, e.g., NHCO indicates the coupling between the NH and CO vibrational band when pump laser pulse is set at the NH vibrational region and probe laser pulse is set at the CO vibrational region. The spectra is normalized to the highest intense peak. In Fig. 3, the spectra is normalized with respect to the carboxyl (C=O) band, which has the highest intensity. All the experiments are performed at room temperature ($21\,^\circ$C).

Figure 3 displays the broad band two-dimensional vibrational echo spectra of 2-Pyrrolidinone in carbon tetrachloride (CCl_4) at population time T_w = 200 fs. One dimensional FTIR spectra of 2-Pyrrolidinone is plotted along with the 2DIR spectra for better understanding of the peak positions and their identification. The spectral range covers the amide-I band (mainly C=O stretch vibrational band at $1700\,cm^{-1}$) and the NH stretch vibrational band[45] at $3250\,cm^{-1}$. Since the pulse width of the IR light is approximately 100 fs, as measured by three beam cross-correlation of a non-resonant solvent sample, it is expected that at population time 200 fs, there would be no contribution from the non-resonant signal. There is a very strong positive peak (red peak) at the lower left side ($\omega_\tau = \omega_m = 1700\,cm^{-1}$) of the broadband spectra. This positive peak is caused by the ground state bleaching and stimulated emission of the CO double bond vibration. The peak is stretched out along the diagonal due to the inhomogeneous broadening. The broadening is a typical feature for such rather short waiting time[46]. A negative peak (blue peak) appears little lower ($\omega_\tau = 1700\,cm^{-1}$, $\omega_m = 1680\,cm^{-1}$) to the diagonal CO stretch vibrational peak, which is caused by the excited state absorption of the amide-I stretch vibrational band. This peak is also inhomogeneously broadened due to the

early waiting time. The positive and the negative peaks are separated by $\delta\omega = \sim 20\,cm^{-1}$ only, as a result, some part of them are overlapped and the peak shapes are deformed. Since water molecules can not be removed completely from the air, some of the IR light is absorbed by them at around $1700\,cm^{-1}$ (which is close to the carbonyl stretch vibrational bond), resulting a gap in the CO vibrational band.
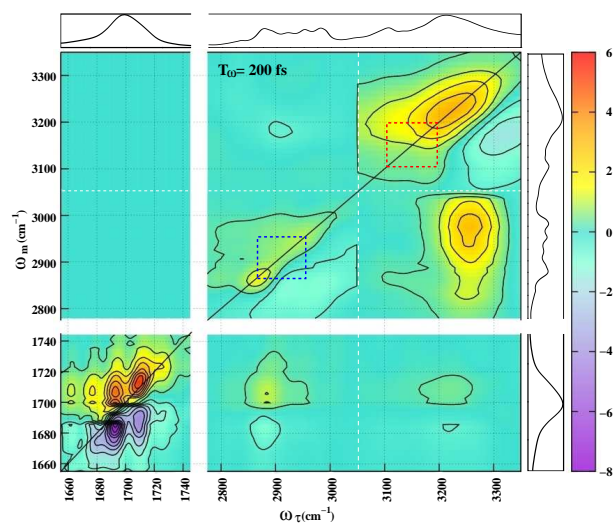

Fig. 3 Two dimensional infrared vibrational photon echo broad band real spectra along with the FTIR spectra of 2-Pyrrolidinone in CCl_4 at a population time $T_w = 200$ fs at room temperature. Two dimensional data have been normalized to the largest peak. The red contours are positive-trending and the blue contours are negative-trending. The horizontal axis is the Fourier transformed τ-axis (ω_τ-axis) and the vertical axis is the monochromator axis (ω_m-axis). The linear FTIR spectra are scaled differently for two different spectral regions.

The next diagonal peak appears in the CH stretch vibration region ($\omega_\tau = \omega_m = 2880\,cm^{-1}$), which corresponds to the ground state bleaching and the excited state emission of the symmetric CH stretch vibration[47]. This peak is much weaker than the amide-I peak. An asymmetric CH stretching mode is also appeared at the diagonal at $\omega_\tau = \omega_m = 2955\,cm^{-1}$, which is rather less intensed. These two peaks are identified as equatorial ($2880\,cm^{-1}$) and axial ($2955\,cm^{-1}$) CH stretch vibrations of the two CH bonds adjacent to the NH group[45]. Both the peaks are stretched out along the diagonal due to the inhomogeneous broadening. A negative peak, parallel to the diagonal, is observed at around ($\omega_\tau = 2960\,cm^{-1}$, $\omega_m = 2810\,cm^{-1}$), caused by the excited state absorption of the symmetric and asymmetric CH stretch vibration bond. This negative peak is stretched out parallel to the diagonal and leading to the inhomogeneous broadening.

A very broad and strong positive peak appears on the diagonal at the amide-A stretch vibrational region. This positive peak is caused by the ground state bleaching and excited state emission of the hydrogen bonded amide-A[45,48] stretch vibration ($\omega_\tau = \omega_m = 3225\,cm^{-1}$). Since at the normal thermal condition, hydrogen bonded chains are randomly distributed in size and different size chains possess different amide-A vibrational frequencies, as a re-

sult a very broad spectral distribution is observed[49–51]. Amide-A band from the shorter chains are appeared at the higher wave number where as from the longer chains, peaks are more in red side of the spectrum. A very weak but never the less a observable peak is appeared on the diagonal at ($\omega_\tau = \omega_m = 3106 \, cm^{-1}$). This peak is due to the ground state bleaching and the excited state emission of the amide-A band from doubly hydrogen bonded dimers (DHBD). A detail of this broadband spectra is explained in a separate paper[45]. A negative peak (blue peak at around $\omega_\tau = 3310 \, cm^{-1}$, $\omega_m = 3180 \, cm^{-1}$) is observed at the NH stretch vibrational region. The negative peak is due to the excited state absorption of the hydrogen bonded NH stretch vibrational mode. This negative peak is stretched out parallel to the diagonal and inhomogeneously broadened. A deformation of this negative peak is observed due to the overlap of a positive peak ($\omega_\tau = 3200 \, cm^{-1}$, $\omega_m = 3106 \, cm^{-1}$) which arises at the lower frequency side of this negative peak (explain later).
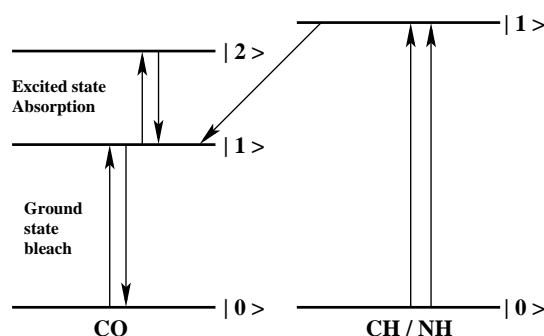

Fig. 4 Energy relaxation from the excited state of the CH/NH vibrational band to the excited state of the CO vibrational band which leads to the incoherent coupling peak in the 2DIR spectra.

Apart from the diagonal peaks, several interesting cross peaks, which are the hallmarks of the 2DIR spectroscopy, are observed in the broad band spectra. In the lower right portion of the spectra, there are two very low intensed positive peaks. They correspond to the coupling between the CH and CO stretch vibrations ($\omega_\tau = 2880 \, cm^{-1}$, $\omega_m = 1710 \, cm^{-1}$) and the coupling between the NH and CO stretch vibrations ($\omega_\tau = 3220 \, cm^{-1}$, $\omega_m = 1710 \, cm^{-1}$). Just bellow to these two positive peaks, there are two negative peaks at ($\omega_\tau = 2880 \, cm^{-1}$, $\omega_m = 1680 \, cm^{-1}$) and ($\omega_\tau = 3220 \, cm^{-1}$, $\omega_m = 1685 \, cm^{-1}$). These peaks are due to the excited state absorption of the CO vibrational bond, which are incoherently coupled with the CH and the NH vibrational band respectively (see Fig. 4). The higher intensity of the CH-CO cross peak than the NH-CO cross peak indicates that the CO vibrational band has stronger coupling with the CH vibrational band than the NH vibrational band. In general cross peaks form a square pattern along with the corresponding diagonal peaks, as a result it is expected to observe a cross peak at the CO pump and the CH/NH probe region (upper left of the spectrum). The question arises why only the CO probe region exhibits the cross peaks but not in the CO pump and the CH/NH probe region? The possible explanation is the incoherent coupling[20,52]: where energy flow from the higher frequency CH and NH vibrational mode to the lower frequency CO vibrational

mode. Since the CH and the NH vibrational bands are higher in energy than the CO vibrational band, the energy relaxation is only possible from the CH and NH to the CO vibrational band, not on the other way (see Fig. 4). As a result pumping at the CO and probing at CH or NH does not give any coupling peak.

A handful of structural information have been observed in the CH and the NH stretch vibrational region. There is a small square feature (blue dotted square in Fig. 3) at the CH vibrational region, which indicates that the axial and equatorial CH stretching modes are coherently coupled to each other and leading to a positive cross peak at ($\omega_\tau = 2880 \, cm^{-1}$, $\omega_m = 2955 \, cm^{-1}$). A similar positive cross peak is expected at the opposite corner of the square, but the peak is covered by the strong negative peak due to the excited state absorption of the CH stretch vibrational band.
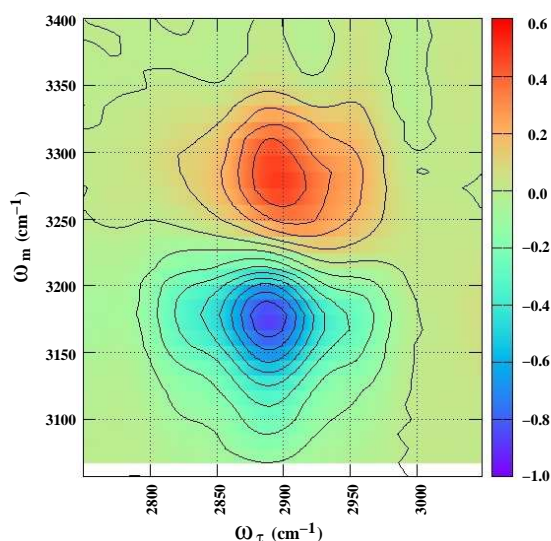
Fig. 5 Coherent coupling peak of the CH and NH vibrational band. The spectra is normalized to the highest peak in the CHNH spectral region.

Another cross peak region is the coupling between the CH and the NH vibrational modes. Apparently there is no prominent cross peak feature is observed at the CHNH coupling region in Fig. 3. An unclear cross peak is only observed at around ($\omega_\tau = 2880 \, cm^{-1}$, $\omega_m = 3180 \, cm^{-1}$). But when the spectra is zoomed and scaled to the highest peak only in the CHNH spectral region, a clear cross peak pattern is observed (see Fig. 5). A positive peak centered at around ($\omega_\tau = 2880 \, cm^{-1}$, $\omega_m = 3250 \, cm^{-1}$) is a clear indication of the coherent coupling between the symmetric CH and the NH vibrational band. The asymmetric CH vibrational band may not couple or has a very small coupling with the NH vibrational band, as a result no observable cross peak is arised due to the asymmetric CH vibration. The positive peak is elongated vertically but due to the negative cross peak at around ($\omega_\tau = 2880 \, cm^{-1}$, $\omega_m = 3180 \, cm^{-1}$), the lower portion of the positive peak is deformed. The vertical elongation of the positive peak indicates that the symmetric CH band always coupled with the NH vibrational band irrespective of the chain size. The negative cross peak at around ($\omega_\tau = 2880 \, cm^{-1}$, $\omega_m = $

3180 cm^{-1}) is due to the coupling between the excited state CH and the NH vibrational band. It is expected that, there should be another positive peak at the NHCH coupling region due to coherent coupling between the NH and the CH vibrational band. But another strong positive broad peak (explain later) covers the NH-CH coherent coupling peak and is not appeared in the 2D plot.

There is a rather strong positive peak at the NHCH coupling region around ($\omega_\tau = 3250$ cm^{-1}, $\omega_m = 2955$ cm^{-1}). This peak is due to the combination of two processes, (i) the coherent coupling between the NH and the CH vibrational band and (ii) the incoherent coupling due to the energy relaxation from the high frequency NH vibrational band to the lower frequency CH vibrational band. Since the NH vibrational band is higher in energy than the CH vibrational band, energy flow is possible from the NH to the CH vibrational band not the other way, as a result there is no incoherent coupling peak is observed at the CHNH coupling region. The higher signal strength at the upper portion of this vertically elongated positive peak indicates that energy flow is favorable to the asymmetric CH vibrational band rather than to the symmetric vibrational band.

An another characteristics square feature (red doted square) is observed to the lower frequency side of the broad amide-A band. A reasonably strong peak is observed at the one corner of the square at around ($\omega_\tau = 3106$ cm^{-1}, $\omega_m = 3200$ cm^{-1}) and the corresponding other cross peak is observed at around ($\omega_\tau = 3200$ cm^{-1}, $\omega_m = 3106$ cm^{-1}). This square feature leading to the hydrogen bond breaking and making mechanism[53] of 2-Pyrrolidinone molecular chain. In one process one of the hydrogen bond from a DHBD breaks and makes another hydrogen bonding with a long chain. In an other process, two 2-Pyrrolidinone molecules together break the hydrogen bonding from one end of the long chain and make a doubly hydrogen bonded dimer. This hydrogen bond making and breaking process is bi-directional and stabilized with the temperature.

4 Conclusions

An experimental methodology is presented to collect the broadband 2DIR spectra of the biological molecules to understand its structure in detail. As a model molecule the cyclic amide, 2-Pyrrolidinone in CCl$_4$ solvent has been studied in detail. The amide-I, amide-A and the hydrogen bonding of 2-Pyrrolidinone, give a clear structural motif of the biological molecule.

A large number of characteristics diagonal and cross peaks are discussed in this article which provide a detail structural information of the molecule. It is well known that due to its large dipole moment the amide-I band remains isolated from the rest of the vibrational bands of the molecule, but the incoherent coupling peaks at the amide-I probe region indicates that energy relaxation can be possible from the higher energy CH and NH vibrational bands to the lower energy CO vibrational band. The square feature in the CH vibrational region gives an indication that the

symmetric and asymmetric CH vibrational bands are coherently coupled. Energy relaxation is also observed from the NH to CH vibrational band which leads to a strong positive incoherent coupling peak at NHCH coupling region. It is observed that single hydrogen bonded oligomers account for the most prominent features in the amide-A region of the vibrational 2DIR spectra. The doubly hydrogen bonded dimer is reflected by relatively weak diagonal peak, which is partly covered by the dominating peak of the oligomers chains. The square feature in the red side of the amide-A band indicates the hydrogen bond making and breaking mechanism between the hydrogen bonded dimers and oligomers. Over all the spectra discussed here provide a significant amount of structural information to understand the molecular structure of the biological molecules in detail.

5 Acknowledgments

References

1 M. Karplus and G. A. Petsko, *Nature*, 1990, **347**, 631.

2 H.-X. Zhou, S. T. Wlodek and J. A. McCammon, *Proc. Nat. Acad. Sci.*, 1998, **95**, 9280–9283.

3 Sobolewski, A. L. and Domcke, W., *Europhys. News*, 2006, **37**, 20–23.

4 C. Scheurer and T. Steinel, *Chem. Phys. Chem.*, 2007, **8**, 503–505.

5 H. Chung and A. Tokmakoff, *Proteins-Structure Function and BioInformatics*, 2008, **72**, 474–487.

6 D. G. Kuroda, J. D. Bauman, J. R. Challa, D. Patel, T. Troxler, E. Das, K. Arnold and R. M. Hochstrasser, *Nature Chemistry*, 2013, **5**, 174–181.

7 *Ultrafast Infrared Vibrational Spectroscopy*, ed. M. D. Fayer, CRC Press, New York and London, 2013.

8 Y. S. Kim and R. M. Hochstrasser, *J. Phys. Chem. B*, 2007, **111**, 9697–9701.

9 Y. S. Kim, L. Liu, P. H. Axelsen and R. M. Hochstrasser, *Pro. Nat. Acd. Sci.*, 2009, **106**, 17751–17756.

10 L. P. DeFlores, Z. Ganim, R. A. Nicodemus and A. Tokmakoff, *J. Am. Chem. Soc.*, 2009, **131**, 3385–3391.

11 M. D. Fayer, *Acc. Chem. Res.*, 2012, **45**, 3–14.

12 K. S. Maiti, *Phys. Chem. Chem. Phys.*, 2015, **17**, 19735–19744.

13 S. Mukamel, *Principles of Nonliner Optical Spectroscopy*, Oxford University Press, New York, 1995.

14 M. Cho, *Two-dimensional optical spectroscopy*, CRC Press, New York and London, 2009.

15 P. Hamm and M. Zanni, *Concepts and Methods of 2D Infrared Spectroscopy*, Cambridge University Press, 2011.

16 P. Hamm, M. Lim and R. M. Hochstrasser, *J. Phys. Chem. B*, 1998, **102**, 6123–6138.

17 S. Borman, *Chem. Eng. News*, 2000, **78**, 41–50.

18 D. M. Jonas, *Science*, 2003, **300**, 1515–1517.

19 T. Steinel, J. B. Asbury, J. Zheng and M. D. Fayer, *J. Phys.*

Chem. A, 2004, **108**, 10957–10964.

20 R. M. Hochstrasser, *Proc. Nat. Acad. Sci.*, 2007, **104**, 14190–14196.

21 A. Tokmakoff, *Science*, 2007, **317**, 54–55.

22 M. T. Zanni, N.-H. Ge, Y. S. Kim and R. M. Hochstrasser, *Proc. Nat. Acad. Sci.*, 2001, **98**, 11265–11270.

23 J. B. Asbury, T. Steinel and M. D. Fayer, *Chem. Phys. Lett.*, 2003, **381**, 139 – 146.

24 J. B. Asbury, T. Steinel, C. Stromberg, S. A. Corcelli, C. P. Lawrence, J. L. Skinner and M. D. Fayer, *J. Phys. Chem. A*, 2004, **108**, 1107–1119.

25 S. A. Corcelli, C. P. Lawrence, J. B. Asbury, T. Steinel, M. D. Fayer and J. L. Skinner, *J. Chem. Phys.*, 2004, **121**, 8897–8900.

26 M. Cho, *Chem. Rev.*, 2008, **108**, 1331–1418.

27 D. M. Jonas, *Annu. Rev. Phys. Chem.*, 2003, **54**, 425–463.

28 P. Tian, D. Keusters, Y. Suzaki and W. S. Warren, *Science*, 2003, **300**, 1553–1555.

29 O. Golonzka, M. Khalil, N. Demirdöven and A. Tokmakoff, *Phys. Rev. Lett.*, 2001, **86**, 2154–2157.

30 N. T. Hunt, *Chem. Soc. Rev.*, 2009, **38**, 1837–1848.

31 P. F. Tekavec, J. A. Myers, K. L. M. Lewis, F. D. Fuller and J. P. Ogilvie, *Opt. Express*, 2010, **18**, 11015–11024.

32 S. Mukamel and H. J. Bakker, *J. Chem. Phys.*, 2015, **142**, 212101.

33 M. C. Asplund, M. T. Zanni and R. M. Hochstrasser, *Proc. Natl. Acad. Sci.*, 2000, **97**, 8219–8224.

34 S. Bagchi, C. Falvo, S. Mukamel and R. M. Hochstrasser, *J. Phys. Chem. B*, 2009, **113**, 11260–11273.

35 P. Hamm, *Structure*, 2009, **17**, 149–150.

36 P. Hamm, J. Helbing and J. Bredenbeck, *Ann. Rev. Phys. Chemi.*, 2008, **59**, 291–317.

37 C. R. Baiz, C. S. Peng, M. E. Reppert, K. C. Jones and A. Tok-

makoff, *Analyst*, 2012, **137**, 1793–1799.

38 C. Greve, N. K. Preketes, H. Fidder, R. Costard, B. Koeppe, I. A. Heisler, S. Mukamel, F. Temps, E. T. J. Nibbering and T. Elsaesser, *J. Phys. Chem. A*, 2013, **117**, 594–606.

39 J. Ono, S. Takada and S. Saito, *J. Chem. Phys.*, 2015, **142**, 212404.

40 M. M. Enriquez, P. Akhtar, C. Zhang, G. Garab, P. H. Lambrev and H.-S. Tan, *J. Chem. Phys.*, 2015, **142**, 212432.

41 S. Shim and M. Zanni, *Phys. Chem. Chem. Phys.*, 2009, **11**, 748–761.

42 M. Bradler, C. Homann and E. Riedle, *Opt. Lett.*, 2011, **36**, 4212–4214.

43 H. Bian, J. Li, X. Wen, Z. Sun, J. Song, W. Zhuang and J. Zheng, *J. Phys. Chem. A*, 2011, **115**, 3357–3365.

44 S. M. G. Faeder and D. M. Jonas, *J. Phys. Chem. A*, 1999, **103**, 10489–10505.

45 K. S. Maiti, A. Samsonyuk, C. Scheurer and T. Steinel, *Phys. Chem. Chem. Phys.*, 2012, **14**, 16294–16300.

46 M. Khalil, N. Demirdöven and A. Tokmakoff, *J. Phys. Chem. A*, 2003, **107**, 5258–5279.

47 D. P. McDermott, *J. Phys. Chem.*, 1986, **90**, 2569–2574.

48 P. B. Petersen, S. T. Roberts, K. Ramasesha, D. G. Nocera and A. Tokmakoff, *J. Phys. Chem. B*, 2008, **112**, 13167–13171.

49 T. Steinel, J. B. Asbury, S. A. Corcelli, C. P. Lawrence, J. L. Skinner and M. D. Fayer, *Chem. Phys. Lett.*, 2004, **386**, 295–300.

50 T. Elsaesser, N. Huse, J. Dreyer, J. R. Dwyer, K. Heyne and E. Nibbering, *Chem. Phys.*, 2007, **341**, 175 – 188.

51 H. Fidder, M. Yang, E. T. J. Nibbering, T. Elsaesser, K. Röttger and F. Temps, *J. Phys. Chem. A*, 2013, **117**, 845–854.

52 S. Gnanakaran and R. M. Hochstrasser, *J. Am. Chem. Soc.*, 2001, **123**, 12886–12898.

53 Y. S. Kim and R. M. Hochstrasser, *Proc. Nat. Acad. Sci.*, 2005, **102**, 11185–11190.